Synthesis of allylamine plasma polymer films: correlation between plasma diagnostic and film characteristics

Laurent Denis,[*a] *Damien Cossement,*[b] *Thomas Godfroid,*[b] *Fabian Renaux,*[b] *Carla Bittencourt,*[a] *Rony Snyders,*[a,b] *and Michel Hecq*[a,b]

[a]Laboratoire de Chimie Inorganique et Analytique, Université de Mons-Hainaut, Place du Parc 20, B-7000 Mons, Belgium.

[b]Materia Nova Research Center, Parc Initialis, Avenue N. Copernic 1, B-7000 Mons, Belgium.

[*] Corresponding author: Tel: +32(0)65373851, Fax: +32(0)65373841, E-mail: laurent.denis@umh.ac.be

Summary

Primary amine-based plasma polymer films (NH_2-PPF) were synthesized using plasma polymerization of allylamine in continuous wave (CW) and pulsed radio-frequency modes. Plasma chemistry, studied by residual gas analysis mass spectrometry, revealed that the fragmentation of the chemical precursor is a function of the equivalent power (P_{eq}), independently of the plasma mode used. X-ray photoelectron spectroscopy combined with time-of-flight secondary ion mass spectrometry suggest as the precursor fragmentation in the plasma increases: (i) a decrease of the primary amines concentration in the NH_2-PPF ($\%NH_2$) and (ii) an increase of the cross-linking degree. Additionally, for a given P_{eq}, the NH_2-PPF characteristics were found to be independent of the plasma mode used. Therefore, the main advantage of using pulsed RF processes over CW ones is the possibility to work at very low P_{eq} what enables low precursor fragmentation, optimization of $\%NH_2$ and reduction of the film cross-linking degree. The chemical composition and the cross-linking degree of the NH_2-PPF synthesized by allylamine plasma polymerization can thus be tailored by adjusting the equivalent RF power injected in the plasma.

Keywords

plasma polymerization, mass spectrometry, derivatization, ESCA/XPS, secondary-ion mass spectrometry (SIMS)

1. Introduction

Plasma polymerization is an attractive method to synthesize organic thin films referred to as "plasma polymer films" (PPF). PPF present, among other properties, strong adherence on numerous surfaces, good mechanical properties and high thermal resistance [1]. Among the most promising PPF, films containing primary amines (NH_2-PPF) have drawn a lot of interest due to their potential applications ranging from modification of membranes [2-8], treatment of polymeric beads [9,10] and carbon nanotubes [11] to biomedical applications [12-18]. Moreover, NH_2-PPF have been reported to exhibit relatively good chemical stability to repeated autoclave cycles and thus resistance to material sterilization, an essential step in the biomedical research and practice [19]. Several nitrogen-rich organic precursors have been considered for NH_2-PPF synthesis [20-25]. Among them, allylamine (CH_2=CH-CH_2-NH_2) has extensively been studied since it contains a carbon-carbon double bond susceptible to polymerize through plasma activation [4,6-10,13-19,22,25-31].

Originally, plasma polymerization was mainly focused on the synthesis of highly cross-linked films with chemical structure featuring little or no repeating monomer units. In the last years, however, this technique has shown its strong potential to modify surface properties of different materials with defined chemical groups. As a consequence, the search for PPF with controllable and stable chemical composition has triggered the last developments in the pulsed plasma polymerization area [15]. For instance, power modulation in pulsed plasma deposition processes allows for a better control over substrate temperature, organic precursor fragmentation in the plasma and physico-chemical properties of the films [32,33]. This modulation is defined by the duty cycle (Δ) giving the relationship between the plasma on-time (τ_{on}, time during which (re)active species and photons are generated) and the

pulse period (sum of τ_{on} and the plasma off-time, τ_{off}, time during which the plasma is switched off).

$$\Delta = \tau_{on} / (\tau_{on} + \tau_{off}) \quad (1)$$

The equivalent power (P_{eq}) is defined as:

$$P_{eq} = \Delta \cdot P_{peak} \quad (2)$$

where, P_{peak} is the input power during the plasma on-time. Relatively high peak powers may frequently be employed but P_{eq} are usually low [33]. Power modulation in pulsed plasma deposition processes, which is proportional to the duty cycle, has often been used to control the retention of the organic precursor chemical group in the PPF [19,26,32]. Under such synthesis conditions, the organic precursor fragmentation increases by increasing P_{eq}. Nevertheless, even when very low P_{eq} is used, the PPF chemistry is difficult to control because, as a consequence of the different chemical reactions occurring during plasma polymerization, a large variety of chemical functions can be incorporated in the PPF. Their nature and relative concentration depend on the organic precursor as well as on the discharge parameters. For instance, it has been shown that allylamine PPF can contain different nitrogen-based chemical functions such as amines, imines and nitriles groups, their relative concentration depending on the experimental conditions [14,27,28,31].

Among the techniques used for quantifying the chemical composition of solids and molecules, X-ray Photoelectron Spectroscopy (XPS) is a powerful well-established method [34]. Nevertheless, in the case of allylamine PPF where different nitrogen-based functions are

present, overlapping of contributions in the X-ray photoemission spectrum is likely. For example, the reported values for the chemical shift of the sp^3-hybridized C-N bonds range from 398 to 398.5 eV; for sp^2-hybridized C=N bonds from 400 to 401 eV; and for sp-hybridized C≡N bonds from 398 to 400 eV [35,36]. Therefore, advanced analysis methods have to be used for a meaningful identification and quantification of chemical groups. Among the potential methods, a combination of XPS with chemical derivatization appears to be a good candidate. It consists in inducing a chemical reaction between a targeted chemical group of the PPF and a chemical reactant containing at least one atom different from the ones composing the PPF. Photoelectrons emitted from the element newly introduced can then be used to quantify the targeted group. For selectively probe $–NH_2$ groups, several reactants such as 4-trifluoromethyl-benzaldehyde (TFBA) [21,37], pentafluoro-benzaldehyde (PFBA) [23] and para-chlorobenzaldehyde [38] have been used.

As mentioned before, the synthesis conditions for deposition of PPF with high primary amines concentration are characterized by low precursor fragmentation. Another consequence of such experimental conditions is the reduction of the PPF cross-linking degree [39]. And yet, it has been shown that the control of the cross-linking degree is an important factor for the optimization of the PPF mechanical and thermal properties [39,40]. Therefore, it is important to evaluate the cross-linking degree in addition to the plasma and PPF chemistry. Time-of-Flight Secondary Ion Mass Spectrometry (ToF-SIMS) has been shown to be a powerful tool to probe structural differences in organic materials [41]. Nevertheless, due to the ToF-SIMS spectra complexity, statistic methods such as Principal Component Analysis (PCA) are increasingly used for data analysis [42-48].

In this work aiming to study the synthesis mechanisms of NH_2-PPF, the plasma chemistry is correlated to the film chemical composition and cross-linking degree. Continuous wave (CW) and pulsed radio-frequency plasma polymerization of allylamine were used to synthesize the films. The plasma chemistry was studied by residual gas analysis (RGA) mass spectrometry. The chemical composition of the NH_2-PPF was determined by chemical derivatization XPS using 4-trifluoromethyl-benzaldehyde (TFBA) as labeling molecule while information about microstructure was deduced from ToF-SIMS data supported by PCA analysis.

2. Experimental Part

Allylamine (98+ % purity) was purchased from Acros Organics, Belgium. PPF were deposited on 1cm^2-silicon (100) substrates. Prior to PPF syntheses, substrates were ultrasonically washed in hexane and then rinsed with methanol.

PPF syntheses were carried out in a 350 mm diameter and 450 mm length cylindrical stainless steel vacuum chamber pumped to a residual pressure of 8.10^{-7} Torr by a combination of rotary and turbomolecular pumps connected in series (**Fig. 1**). The 13.56 MHz exciting power was applied via a matching network to a water-cooled copper coil, 150 mm internal diameter and 8 mm tore thickness, located inside the chamber 100 mm in front of the substrate. A load-lock system allows transferring the substrate inside the reactor from atmosphere to high vacuum in few minutes. The introduction airlock is separated of the main chamber by a slide valve. The substrate holder is mounted on a transfer stick and the substrate kept at floating potential during PPF deposition. A full-range gauge allows controlling the

residual pressure before PPF synthesis whereas the process pressure, regulated by a throttle valve located upstream the turbomolecular pump, is given by a Baratron gauge. The organic precursor inlet is placed in front of the substrate. Allylamine flow rate was fixed at 10 sccm during all the experiments and the working pressure regulated at 20 mTorr. Allylamine PPF were synthesized under pulsed and CW power conditions summarized in **Table 1**.

A common feature when dealing with plasma polymerization processes is to determine the PPF deposition regime. For that purpose, the lowest equivalent power condition was considered (30 W). It has been shown, when the plasma is pulsed, that the deposition regime depends only on the average energy dissipated per precursor molecule, E_{mean}, in the plasma [49,50].

$$E_{mean} = \frac{P_{eq}}{N} \cdot \tau_{res} = \Delta \cdot \frac{P_{peak}}{N} \cdot \tau_{res} \quad (3)$$

where N is the number of particles resident in the system and τ_{res} their resident time, given by $\tau_{res} = N/\Phi$, where Φ is the precursor flow rate. Therefore,

$$E_{mean} = \Delta \cdot \frac{P_{peak}}{\Phi} \quad (4)$$

It should be emphasized that relation 4 can only be applied if the residence time is much longer that the pulse period. The calculation of the residence time requires the determination of N and expression of Φ in number of molecules per second. In our system, the allylamine flow rate was fixed at 10 sccm corresponding to 4.5×10^{18} molecules per second. On the other hand, at a process pressure of 2.67 Pa and for a chamber volume of ~ 4.33×10^{-2} m^3, we obtain

$N = 2.8 \times 10^{19}$ molecules resident every time in the chamber. This gives a residence time of 6.2 s which is much longer than the pulse period of our experiment namely 1.9 msec. An absorbed power of 1 W/sccm of precursor flow rate corresponds to 15.5 eV of average energy dissipated per precursor molecule in the plasma [49,50]. For P_{eq} = 30 W, we have E_{mean} = 3 W/sccm (46.5 eV/molecule), this value being consistent with a monomer deficient regime [51].

Plasma composition was investigated by residual gas analysis (RGA) mass spectrometry. The mass spectrometer is a quadrupole HAL EQP 500 model supplied by Hiden Analytical (Warrington, UK). The apparatus is interfaced to the chamber by a 100 µm extraction orifice located between the coil and the substrate holder. Prior to detection, neutral species were ionized by electron impact with an electron kinetic energy fixed at 20 eV in order to limit additional fragmentations in the ion source [52-54]. It should be noted that the mass spectrometer quadrupole is a mass-dependent system whose transmission function decreases strongly with the studied mass, m. The manufacturer of the HAL EQP 500 has found empirically that this mass-dependent instrument function ranges between m^{-1} and m^{-2}. In this work, we have used a m^{-1} mass-dependent function to correct the spectra [55].

XPS experiments were performed on TFBA-derivatized samples. Data were acquired with a VG-ESCALAB 220iXL spectrometer. A monochromatized Al K_α line (1486.6 eV) was used as photon source. The overall energy resolution was 0.6 eV. The pressure in the analysis chamber was 1.5×10^{-9} Torr. Surface charging effect was compensated using a 6 eV electron flood gun. Photoemission spectrum background signal was subtracted using the linear method. Elemental composition was deduced from photoelectron peak areas using respective photoionisation cross-section calculated by Scofield [56], corrected by the escape depth

dependence on the electron kinetic energy (assumed to have the form $\lambda = KE^{0.6}$) and by the analyzer transmission function of the spectrometer.

The derivatization reaction was performed by exposing the PPF to TFBA vapor in a separated chamber at 3 Torr pressure and room temperature. **Scheme 1** shows the reaction occurring during the $–NH_2$ groups derivatization. The reaction consists in a nucleophilic addition on carbonyl group (C=O) that converts $–NH_2$ group into imine (Schiff base). Hence, $–NH_2$ groups are selectively probed by the reagent $–CF_3$ terminal group. Kinetics of this reaction was investigated as a function of the PPF synthesis conditions. For these experiments, PPF were TFBA-derivatized using different reaction times. After the derivatization step, $\%NH_2$ was calculated from XPS according to [57]:

$$\%NH_2 = \frac{[NH_2]}{[N]} = \frac{([F]/3)}{[N]}.100\% \qquad (5)$$

where $[NH_2]$, [N] and [F] represent respectively the relative concentration of primary amines, nitrogen and fluorine at the PPF surface. The $[NH_2]/[N]$ ratio is referred to as the process selectivity.

Static ToF-SIMS data of the as-deposited PPF were acquired by a time-of-flight secondary ion mass spectrometer, using a ToF-SIMS IV instrument from ION-TOF GmbH (Münster, Germany). An Ar^+ 10 keV ion beam at a current of 0.2 pA for samples 1 and 2, and 1 pA for samples 3 and 4, rastered over a scan area of 300 μm × 300 μm was used as analysis beam. The detection was made in the positive ion mode. For each spectrum the mass scale was calibrated by using well identified ions namely H^+, H_2^+, H_3^+, C^+, CH^+, CH_2^+, CH_3^+ and $C_2H_3^+$. Five measurements were performed on each sample keeping settings unchanged. The

ToF-SIMS spectra were analyzed by the PCA method using the SIMCA-P11 software supplied by Umetrics, Sweden. The peak intensity of the secondary ions was normalized to the total ion count before performing the PCA to correct for the differences in total secondary ion yield from spectrum to spectrum. The normalized spectra were exported from the acquisition software (IONSPEC v3.16) to the analysis software SIMCA-P11 which mean-centers and scales the variables. This procedure ensures that the variance in the data are related to chemical differences between samples and not to artifacts in peak intensity [44,46].

PCA is a multivariate analysis technique aiming at summarizing the variance patterns within a dataset. The variance in the data describes the differences between samples. In ToF-SIMS data, these differences come from changes in the relative intensity of the peaks within samples spectra. Before data processing, results are set in matrix form where the rows are the samples (i.e. spectra) and the columns are the variables (i.e. peaks). When PCA is applied, a new set of axes (principal components, PCi) is created defining the directions of the major variations within the data set. The result of this is a reduction of variables since the original ones are recombined to define the new PC axis. The large data set is thus reduced to some variables that are interpreted using specific plots. Two main concepts are then introduced namely the scores and the loadings. The scores describe the relationship between samples and account for reproducibility of the surface chemistry results. The loadings define the contributions of the original variables to the new PCi and describe the variables responsible for the differences between the samples [44,46].

3. Results and Discussion

It has been shown that apart from neutral free radical species, positive ion-molecule reactions can also have important influence in the PPF deposition, especially if the plasma polymerization is carried out in CW mode at low input power (~ between 0.5 and 15 W) [58-61]. Under such plasma conditions, the observation of positively charged oligomers in the plasma and the absence of such neutral species suggested a cationic chain polymerization mechanism. During low input power plasma polymerization of acrylic acid, the flux of positive species arriving at the sample surface revealed the positive ion deposition mechanism [62]. Similar experiments, considering low input power plasma polymerization of allylamine, also demonstrated that the ionic mass transported to the surface is sufficient to account for all the deposit [55]. Nevertheless, for power higher than ~ 15 W, an increased fragmentation of the organic precursor associated with the loss of positively charged oligomers is observed in the plasma [63]. Hence, since in this work the power applied in CW or during the plasma on-time was always ≥ 75 W, it can be assumed that the NH_2-PPF growth mechanism occurred via radicalar species reactions. Consequently, we focused the plasma chemistry analysis on neutral particles.

The electron impact mass spectrum of allylamine vapor (without plasma) is shown in **Figure 2** (spectrum 2a). Four major peaks are observed at *m/z* 57, 56, 30 and 28, coming from α-cleavage reactions of the precursor ($[C_3H_7N]^{+\cdot}$). This radical-cation can lose either a hydrogen radical giving the ($[C_3H_6N]^+$) signal at *m/z* 56 or a vinyl radical producing the ($[CH_4N]^+$) signal at *m/z* 30. Subsequent dehydrogenation of the latter yields to ($[CH_2N]^+$) signal at *m/z* 28. Spectra 2b to 2e show the RGA mass spectra of the plasma as a function of the experimental conditions. The spectra were recorded from 1 to 60 m/z because no

significant signal was detected beyond this value. This result suggests that oligomerization reactions involving radicalar species (radical-radical or radical-neutral) rarely occur during the plasma polymerization process. This observation is in good agreement with previous studies reporting RGA mass spectrometry measurements performed on acrylic acid [51], propanoic acid [59] and allyl alcohol [60] plasma neutral species.

The different peaks were assigned as follow: *m/z* 1, 2, 3, ($[H_X]^+$) with X varying from 1 to 3; *m/z* 15, 16, 17, 18, ($[NH_X]^+$) with a contribution from ($[CH_3]^+$), ($[CH_4]^{+\cdot}$) and ($[H_2O]^{+\cdot}$) at *m/z* 15, 16 and 18, respectively; *m/z* 26, ($[CN]^+$) with a contribution from ($[C_2H_2]^{+\cdot}$); *m/z* 28, ($[CH_2N]^+$), ($[C_2H_4]^{+\cdot}$) and a possible contribution from ($[N_2]^{+\cdot}$); *m/z* 30, ($[CH_4N]^+$) with a contribution of ($[C_2H_6]^{+\cdot}$); *m/z* 41 and 42, ($[C_3H_5]^+$) and ($[C_3H_6]^{+\cdot}$), respectively. It is important to mention that even when low P_{eq} (30 W) is used, complete dehydrogenation of the chemical precursor is observed at *m/z* 50. In this region of the spectrum, signals between 58 and 50 *m/z* correspond to molecular fragments of ($[C_3H_XN]^+$) as raw chemical formula, with X varying from 0 to 8. It has been shown that the retention, in the films, of the chemical group hosted by the precursor behaves in the opposite trend towards the molecule fragmentation in the gas-phase [51,61]. As a consequence, it can be expected from these mass spectrometry data that sample 1 contains the highest *%NH₂* since spectrum 2b, corresponding to the latter sample, presents the highest signal at *m/z* = 56. Following the same assumption, sample 4 (spectrum 2e) should present the lowest *%NH₂* while samples 2 and 3, spectrum 2c and 2d respectively, should reveal similar chemistry.

In order to probe *%NH₂*, a combination of XPS and TFBA derivatization was employed. **Figure 3** compares the typical XPS survey spectra of as-deposited (spectrum 3a) and TFBA-derivatized (spectrum 3b) NH_2-PPF. Although allylamine is free of oxygen, an O1s signal at ~ 531.0 eV is observed in both spectra. This is likely the result of post-growth

oxidation processes following film exposure to ambient air [64,65]. For the derivatized sample, appearance of the fluorine (F1s) peak is clearly observed at ~ 685.0 eV. From the analysis of this latter peak, it is possible to calculate $\%NH_2$ as it is mentioned in the experimental part.

Before the data processing, the quantification method was validated. The first step was the study of the derivatization reaction kinetics. **Figure 4** shows the evolution of $\%NH_2$ as a function of the derivatization duration. The saturation in $\%NH_2$ (plateau region) for increasing derivatization time can be attributed to the complete derivatization reaction of the $-NH_2$ groups. The lowest derivatization time is observed for sample 4 (P_{eq} = 175 W) for which $\%NH_2$ saturates after ~ 90 minutes of derivatization. For samples 2 and 3 (P_{eq} = 75 W), complete derivatization reaction requires ~ 240 minutes while for sample 1, synthesized at 30 W, the saturation is reached after ~ 960 minutes of derivatization. Hence, in order to be sure that all $-NH_2$ groups are probed; the latter derivatization time was used for all samples.

In a second step, the depth dependence of the derivatization was probed by modifying the angle of XPS analysis. We found that, taking into account the experimental uncertainty, the NH_2-PPF composition is independent on the analysis angle used confirming that the XPS analysis depth, for the excitation energy used, is smaller than the depth of the derivatized region. As an example, for sample 3, the $\%NH_2$ evaluated using the XPS data recorded at a detection angle (θ) of 90°, 74° and 55° (with reference to the sample surface) were 8.5 ± 1 %, 9.2 ± 1 % and 9.0 ± 1 %.

Table 2 presents the elemental chemical composition of the NH_2-PPF, their $\%NH_2$ and the RGA precursor signal (I_{allyl}) as a function of the synthesis conditions. The results show

that $\%NH_2$ and I_{allyl} increase as P_{eq} decreases. Hence, supporting the assumption based on the RGA data, the sample prepared using the lowest P_{eq} (sample 1) has the highest $\%NH_2$ value while the sample prepared using the highest P_{eq} (sample 4) has the lowest one. The results show the correlation between the precursor fragmentation and the insertion of primary amines groups in the PPF. Furthermore, it can be observed that samples 2 and 3 are similar in terms of chemistry. The latter result is in good agreement with previous studies which have revealed similar primary amines contents and subsequent DNA immobilization properties for allylamine PPF synthesized in similar P_{eq} conditions, the power range being lower than the one studied in this work [13,27].

As already mentioned, in addition to the chemical composition, the PPF cross-linking degree is also affected by the P_{eq} value. Among the numerous parameters influencing the PPF microstructure, E_{mean}/M, with M the precursor molar mass, can be correlated to the precursor fragmentation degree [51,66]. Variation of the power conditions while keeping unchanged the precursor type and flow rate should thus allow the synthesis of PPF with different cross-linking degrees. In order to investigate the cross-linked nature of the PPF prepared using different P_{eq}, the latter were analyzed by ToF-SIMS. **Figure 5** shows the PPF positive ToF-SIMS spectra ranging from m/z = 0 to m/z = 150 as a function of the synthesis conditions. Except for some differences in relative intensity of the peaks, it is difficult to establish specific trends.

In order to extract information related to the chemical structure of the NH_2-PPF, the ToF-SIMS data were processed by PCA. **Figure 6** shows the positive ToF-SIMS data presented in a "scores plot" in which each individual point represents a whole ToF-SIMS spectrum of a given NH_2-PPF. The ellipse drawn on the scores plot is the 95% confidence

interval calculated from Hotelling's T-square statistic [42]. Two principal components (PCi) were identified representing together 80% of the data variance: PC1 represents nearly 62% of the variance while PC2 counts for 18%. The scores plot of PC1 versus PC2, for the PCA model applied to the ToF-SIMS spectra, distributes the samples according to their fragmentation pattern. In the scores plot (**Fig. 6**), the samples 2 and 3 can not be discriminated, what is in accordance with the XPS results suggesting that these samples are chemically similar even if they are synthesized in different plasma mode conditions. In contrast, samples 1 and 4 are clearly discriminated from the other samples.

A scores plot is always associated to a "loadings plot", the negative scores are characterized by the negative loadings and the positive scores by the positive loadings. The loadings reveal the ionized fragments responsible for samples discrimination in the scores plot. **Table 3** shows the PC1 negative and positive loadings whose relative statistical weight in the model is > 90%. From the scores plot (**Fig. 6**), sample 1 is clearly different from the three others having a negative PC1. The characteristic ionized fragments of sample 1, corresponding to the negative loadings of PC1 (**Table 3**), are hydrocarbonated ions ($C_xH_y^+$) and, in bold type (**Table 3**), nitrogen-based ions ($C_xH_yN^+$). On the contrary, for samples 2, 3 and 4, which are characterized by positive values of PC1, the main characteristic ions are hydrocarbonated ($C_xH_y^+$), nitrogen-based ions are not statistically important species.

The presence of nitrogen-based fragments for sample 1 indicates a high content of nitrogen-based chemical groups in the PPF in agreement with the XPS analysis that revealed the highest $\%NH_2$ for this sample synthesized at the lowest P_{eq} (**Table 2**). Additionally, the relative chemical composition of the $C_xH_y^+$ species suggests a lower cross-linking degree for

sample 1 compared to the samples 2, 3 and 4 since the ionized fragments detected for this sample contains an average of 7 carbon atoms compared to 4.5 for samples 2, 3 and 4.

PC1 explains almost 62% of the data variance and clearly discriminates the sample 1 from the others on chemical and structural characteristics. However, distinction between the samples 2, 3 and 4, characterized by a positive PC1, can also be obtained by considering PC2, representing 18% of the variance. Similarly than for PC1, **Table 4** summarizes the most important fragments characterizing the positive and negative values of PC2. Sample 4 is characterized by the negative loadings of PC2 while samples 2 and 3 by the positive ones. The negative PC2 loadings reveal fragments having in average 3 carbon atoms while, for the positive loadings, the number of carbon atoms is equal to 12. This result thus suggests a higher cross-linking degree for sample 4 with regard to samples 2 and 3. Therefore, the latter have similar structure as well as similar chemical composition. Finally, when comparing the characteristic ionized fragments of PC2, it can be observed that only the positive PC2 includes nitrogen-based fragments. This supports the XPS data from which we have deduced a slightly higher $\%NH_2$ for sample 2 and 3 than for sample 4.

4. Conclusions

In this work, CW and pulsed RF plasma polymerization of allylamine were investigated. The plasma chemistry, studied by RGA mass spectrometry, revealed that the allylamine fragmentation is strongly dependent on P_{eq} whatever the plasma is sustained in CW or pulsed mode. In order to evaluate the effect of the precursor fragmentation on the PPF chemistry, a combination of XPS and TFBA derivatization was used. Additionally, the PPF

microstructure was evaluated by identifying the statistically important ionic fragments composing the ToF-SIMS spectra through PCA analysis.

XPS and ToF-SIMS data revealed, as the precursor fragmentation in the plasma increases, a decrease of the primary amines concentration in the NH_2-PPF ($\%NH_2$) while their cross-linking degree increases, the latter behaving in the opposite trend towards the precursor mass signal in the plasma. The use of low P_{eq} enables: (i) low precursor fragmentation, (ii) optimization of the primary amine concentration in the PPF and (iii) reduction of the cross-linking degree. For a given P_{eq}, the plasma mode (CW or pulsed) has no influence on the PPF characteristics. Therefore, the main advantage of using pulsed RF processes is the possibility to work at very low P_{eq} compared to the CW mode.

These findings are of great importance in order to be able to optimize the chemical selectivity of the primary amine-based PPF as well as their cross-linking degree.

Acknowledgements

This work is supported by the « Fonds pour la Formation à la Recherche dans l'Industrie et dans l'Agriculture » (F.R.I.A.) and the Belgian Government through the « Pôle d'Attraction Interuniversitaire» (PAI, P6/08, "Plasma-Surface Interaction", Ψ).

References

[1] **"***Plasma Technology, vol. 3 – Plasma Polymerization Processes"*, H. Biederman, Y. Osada, Eds., Elsevier Science Publishers, Amsterdam 1992.

[2] H. Matsuyama, K. Hirai, M. Teramoto, *J. Membr. Sci.* **1994**, *92*, 257.

[3] R. C. Ruaan, T. H. Wu, S. H. Chen, J. Y. Lai, *J. Membr. Sci.* **1998**, *138*, 213.

[4] H. I. Kim, S. S. Kim, *J. Membr. Sci.* **2001**, *190*, 21.

[5] G. Pozniak, I. Gancarz, M. Bryjak, W. Tylus, *Desalination* **2002**, *146*, 293.

[6] I. Gancarz, G. Pozniak, M. Bryjak, W. Tylus, *Eur. Polym. J.* **2002**, *38*, 1937.

[7] P. Hamerli, Th. Weigel, Th. Groth, D. Paul, *Biomaterials* **2003**, *24*, 3989.

[8] P. Hamerli, Th. Weigel, Th. Groth, D. Paul, *Surf. Coat. Technol.* **2003**, *174-175*, 574.

[9] G. Oye, V. Roucoules, A. M. Cameron, L. J. Oates, N. R. Cameron, P. G. Steel, J. P. S. Badyal, B. G. Davis, D. Coe, R. Cox, *Langmuir* **2002**, *18*, 8996.

[10] G. Oye, V. Roucoules, L. J. Oates, A. M. Cameron, N. R. Cameron, P. G. Steel, J. P. S. Badyal, B. G. Davis, D. M. Coe, R. A. Cox, *J. Phys. Chem. B* **2003**, *107*, 3496.

[11] Q. Chen, L. Dai, M. Gao, S. Huang, A. Mau, *J. Phys. Chem. B* **2001**, *105*, 618.

[12] L. Dai, H. A. W. StJohn, J. Bi, P. Zientek, R. C. Chatelier, H. J. Griesser, *Surf. Interface Anal.* **2000**, *29*, 46.

[13] Z. Zhang, Q. Chen, W. Knoll, R. Foerch, R. Holcomb, D. Roitman, *Macromolecules* **2003**, *36*, 7689.

[14] Q. Chen, R. Förch, W. Knoll, *Chem. Mat.* **2004**, *16*, 614.

[15] R. Förch, Z. Zhang, W. Knoll, *Plasma Process. Polym.* **2005**, *2*, 351.

[16] Z. Zhang, W. Knoll, R. Förch, *Surf. Coat. Technol.* **2005**, *200*, 993.

[17] T. B. Ren, Th. Weigel, Th. Groth, A. Lendlein, *J. Biomed. Mater. Res. Part A* **2008**, *86A*, 209.

[18] A. L. Hook, H. Thiessen, J. Quinton, N. Voelcker, *Surf. Sci.* **2008**, *602*, 1883.

[19] A. Harsch, J. Calderon, R. B. Timmons, G. W. Gross, *J. Neurosci. Methods* **2000**, *98*, 135.

[20] T. R. Gengenbach, H. J. Griesser, *J. Polym. Sci. Pol. Chem.* **1999**, *37*, 2191.

[21] A. Choukourov, H. Biederman, D. Slavinska, M. Trchova, A. Hollander, *Surf. Coat. Technol.* **2003**, *174-175*, 863.

[22] A. G. Shard, J. D. Whittle, A. J. Beck, P. N. Brookes, N. A. Bullett, R. A. Talib, A. Mistry, D. Barton, S. L. McArthur, *J. Phys. Chem. B* **2004**, *108*, 12472.

[23] J. Kim, D. Jung, Y. Park, Y. Kim, D. W. Moon, T. G. Lee, *Appl. Surf. Sci.* **2007**, *253*, 4112.

[24] Y. Martin, D. Boutin, P. Vermette, *Thin Solid Films* **2007**, *515*, 6844.

[25] G. S. Malkov, I. T. Martin, W. B. Schwisow, J. P. Chandler, B. T. Wickes, L. J. Gamble, D. G. Castner, E. R. Fisher, *Plasma Process. Polym.* **2008**, *5*, 129.

[26] H. Schönherr, M. T. van Os, R. Förch, R. B. Timmons, W. Knoll, G. J. Vancso, *Chem. Mat.* **2000**, *12*, 3689.

[27] A. Choukourov, H. Biederman, D. Slavinska, L. Hanley, A. Grinevich, H. Boldyryeva, A. Mackova, *J. Phys. Chem. B* **2005**, *109*, 23086.

[28] M. Tatoulian, F. Bretagnol, F. Arefi-Khonsari, J. Amouroux, O. Bouloussa, F. Rondelez, A. J. Paul, R. Mitchell, *Plasma Process. Polym.* **2005**, *2*, 38.

[29] U. Oran, S. Swaraj, A. Lippitz, W. E. S. Unger, *Plasma Process. Polym.* **2006**, *3*, 288.

[30] S. Igarashi, A. N. Itakura, M. Toda, M. Kitajima, L. Chu, A. N. Chifen, R. Förch, R. Berger, *Sens. Actuator B - Chem.* **2006**, *117*, 43.

[31] M. Lejeune, F. Bretagnol, G. Ceccone, P. Colpo, F. Rossi, *Surf. Coat. Technol.* **2006**, *200*, 5902.

[32] C. R. Savage, R. B. Timmons, J. W. Lin, *Chem. Mat.* **1991**, *3*, 575.

[33] R. B. Timmons, A. J. Griggs, "Pulsed Plasma Polymerizations", in: *Plasma Polymer Films*, H. Biederman, Ed., Imperial College Press, London 2004.

[34] "*Photoelectron Spectroscopy: Principles and Applications"*, 3rd edition, S. Hüfner, Ed., Springer, Berlin 2003.

[35] A. K. M. S. Chowdhury, D. C. Cameron, M. S. J. Hashmi, *Surf. Coat. Technol.* **1999**, *112*, 133.

[36] D. Q. Yang, E. Sacher, *Surf. Sci.* **2003**, *531*, 185.

[37] I. Losito, E. De Giglio, N. Cioffi, C. Malitesta, *J. Mater. Chem.* **2001**, *11*, 1812.

[38] R. Snyders, O. Zabeida, C. Roberges, K. I. Shingel, M. P. Faure, L. Martinu, J. E. Klemberg-Sapieha, *Surf. Sci.* **2007**, *601*, 112.

[39] R. Prikryl, V. Cech, L. Zajickova, J. Vanek, S. Behzadi, F. R. Jones, *Surf. Coat. Technol.* **2005**, *200*, 468.

[40] D. D. Burkey, K. K. Gleason, *Chem. Vapor Depos.* **2003**, *9*, 65.

[41] L. Lianos, C. Quet, T. M. Duc, *Surf. Interface Anal.* **1994**, *21*, 14.

[42] M. S. Wagner, D. G. Castner, *Langmuir* **2001**, *17*, 4649.

[43] M. von Gradowski, M. Wahl, R. Förch, H. Hilgers, *Surf. Interface Anal.* **2004**, *36*, 1114.

[44] M. S. Wagner, D. J. Graham, B. D. Ratner, D. G. Castner, *Surf. Sci.* **2004**, *570*, 78.

[45] M. von Gradowski, B. Jacoby, H. Hilgers, J. Barz, M. Wahl, M. Kopnarski, *Surf. Coat. Technol.* **2005***, 200*, 334.

[46] D. J. Graham, M. S. Wagner, D. G. Castner, *Appl. Surf. Sci.* **2006**, *252*, 6860.

[47] B. J. Tyler, *Appl. Surf. Sci.* **2006**, *252*, 6875.

[48] B. J. Tyler, G. Rayal, D. G. Castner, *Biomaterials* **2007**, *28*, 2412.

[49] M. Bauer, T. Schwarz-Selinger, H. Kang, A. von Keudell, *Plasma Sources Sci. Technol.* **2005**, *14*, 543.

[50] M. Bauer, T. Schwarz-Selinger, W. Jacob, A. von Keudell, *J. Appl. Phys.* **2005**, *98*, 073302.

[51] S. A. Voronin, M. Zelzer, C. Fotea, M. R. Alexander, J. W. Bradley, *J. Phys. Chem. B* **2007**, *111*, 3419.

[52] "*Cold Plasma in Materials Fabrication – From Fundamentals to Applications*", A. Grill, Ed., IEEE Press, New York 1994.

[53] M. J. Vasile, G. Smolinsky, *Int. J. Mass Spectrom.* **1976**, *21*, 263.

[54] R. Manory, A. Grill, U. Carmi, R. Avni, *Plasma Chem. Plasma Process.* **1983**, *3*, 235.

[55] A. J. Beck, S. Candan, R. D. Short, A. Goodyear, N. St J. Braithwaite, *J. Phys. Chem. B* **2001**, *105*, 5730.

[56] J. H. Scofield, *J. Electron Spectrosc. Relat. Phenom.* **1976**, *8*, 129.

[57] F. Truica-Marasescu, M. R. Wertheimer, *Plasma Process. Polym.* **2008**, *5*, 44.

[58] D. B. Haddow, R. M. France, R. D. Short, J. W. Bradley, D. Barton, *Langmuir* **2000**, *16*, 5654.

[59] L. O'Toole, A. J. Beck, A. P. Ameen, F. R. Jones, R. D. Short, *J. Chem. Soc. Faraday Trans.* **1995**, *91*, 3907.

[60] L. O'Toole, C. A. Mayhew, R. D. Short, *J. Chem. Soc. Faraday Trans.* **1997**, *93*, 1961.

[61] L. O'Toole, R. D. Short, *J. Chem. Soc. Faraday Trans.* **1997**, *93*, 1141.

[62] S. Candan, A. J. Beck, L. O'Toole, R. D. Short, A. Goodyear, N. St J. Braithwaite, *Phys. Chem. Chem. Phys.* **1999**, *1*, 3117.

[63] M. R. Alexander, F. R. Jones, R. D. Short, *J. Phys. Chem. B* **1997**, *101*, 3614.

[64] T. R. Gengenbach, Z. R. Vasic, R. C. Chatelier, H. J. Griesser, *J. Polym. Sci. Pol. Chem.* **1994**, *32*, 1399.

[65] T. R. Gengenbach, Z. R. Vasic, S. Li, R. C. Chatelier, H. J. Griesser, *Plasmas Polym.* **1997**, *2*, 91.

[66] "*Plasma Polymerization"*, H. Yasuda, Ed., Academic Press, Orlando 1985.

List of Figures

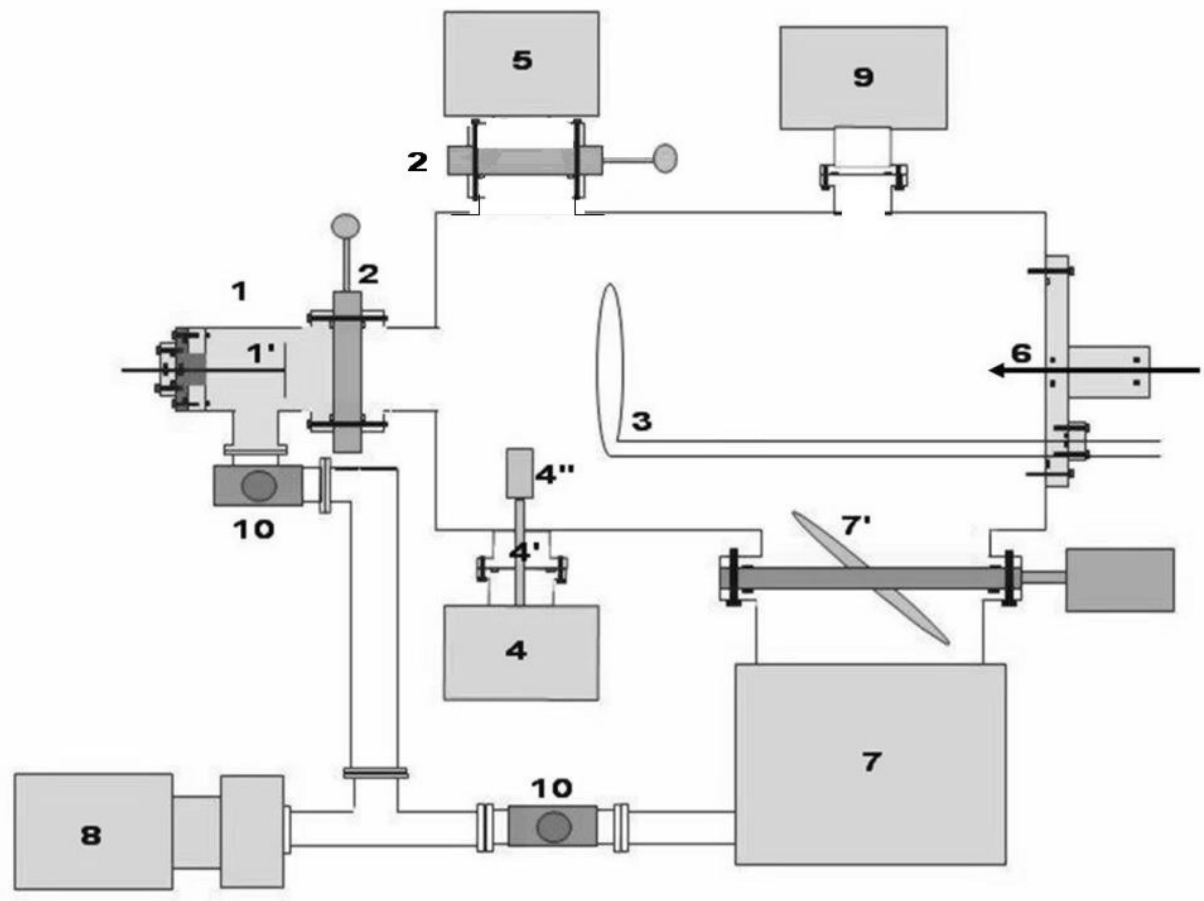

Figure 1

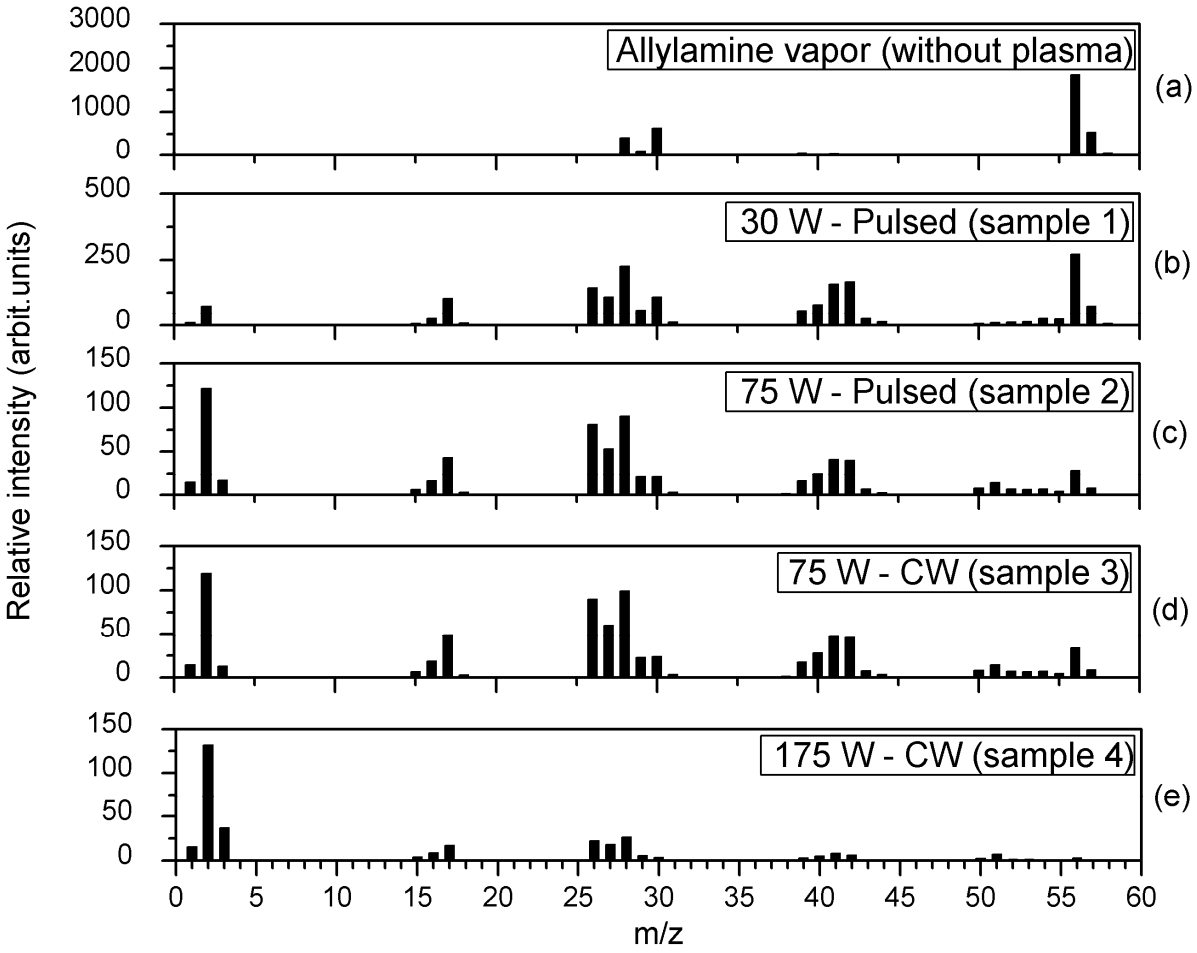
Allylamine vapor (without plasma)
(a)
30 W - Pulsed (sample 1)
(b)
75 W - Pulsed (sample 2)
(c)
75 W - CW (sample 3)
(d)
175 W - CW (sample 4)
(e)
Relative intensity (arbit.units)
m/z
3000
2000
1000
0
500
250
150
100
50
0
0
5
10
15
20
25
30
35
40
45
50
55
60

Figure 2

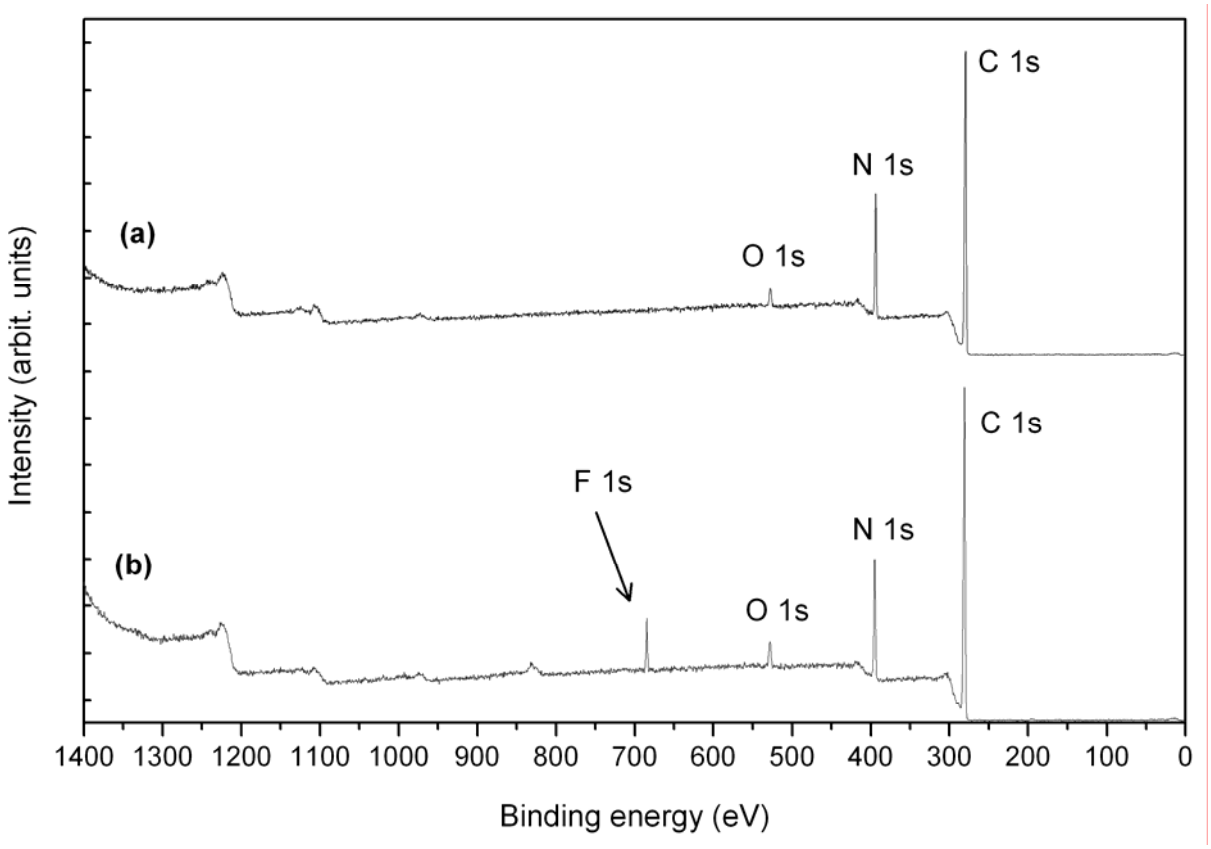
C 1s
N 1s
(a)
O 1s
C 1s
F 1s
N 1s
(b)
O 1s
Intensity (arbit. units)
1400 1300 1200 1100 1000 900 800 700 600 500 400 300 200 100 0
Binding energy (eV)

Figure 3

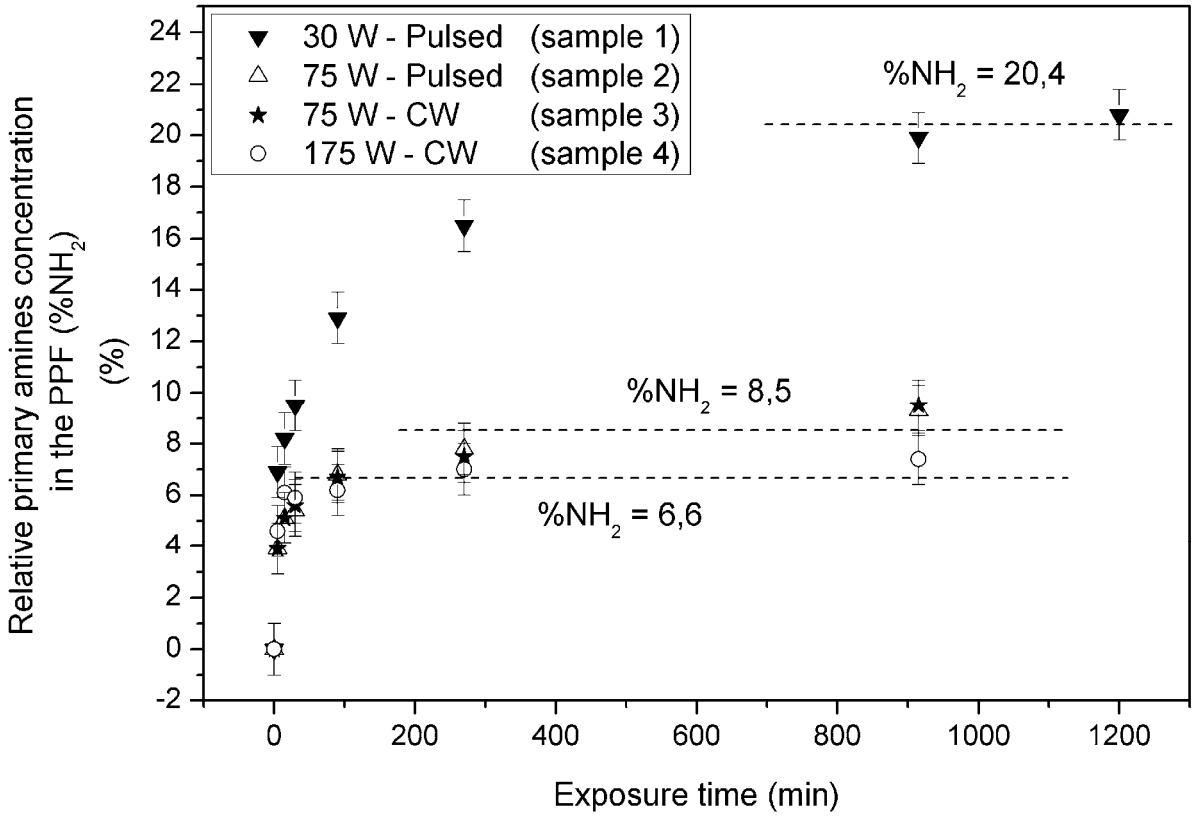
30 W - Pulsed (sample 1)
75 W - Pulsed (sample 2)
75 W - CW (sample 3)
175 W - CW (sample 4)
%NH2 = 20,4
%NH2 = 8,5
%NH2 = 6,6
Relative primary amines concentration in the PPF (%NH2) (%)
Exposure time (min)
24
22
20
18
16
14
12
10
8
6
4
2
0
-2
0
200
400
600
800
1000
1200

Figure 4

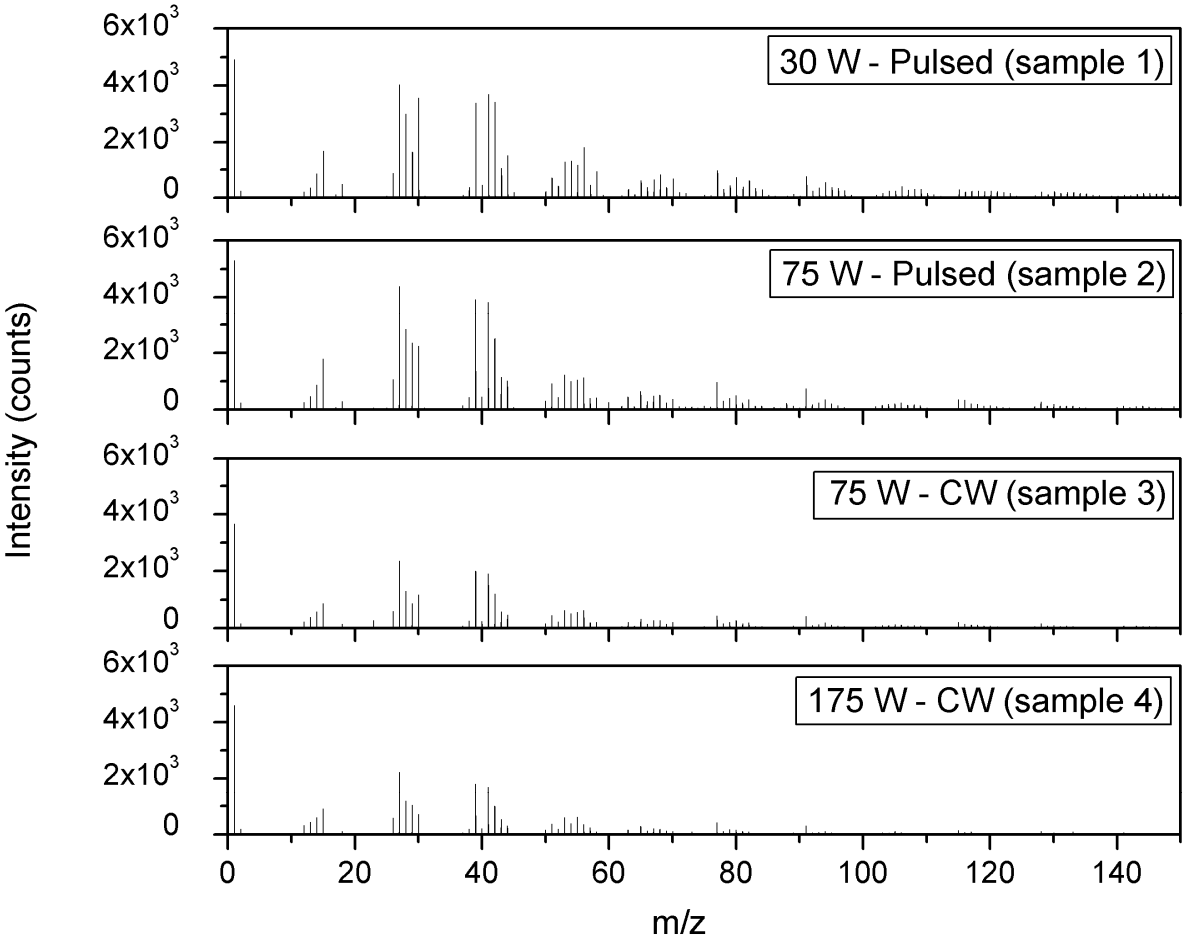
Intensity (counts)
6x10^3
4x10^3
2x10^3
0
30 W - Pulsed (sample 1)
75 W - Pulsed (sample 2)
75 W - CW (sample 3)
175 W - CW (sample 4)
0
20
40
60
80
100
120
140
m/z

Figure 5

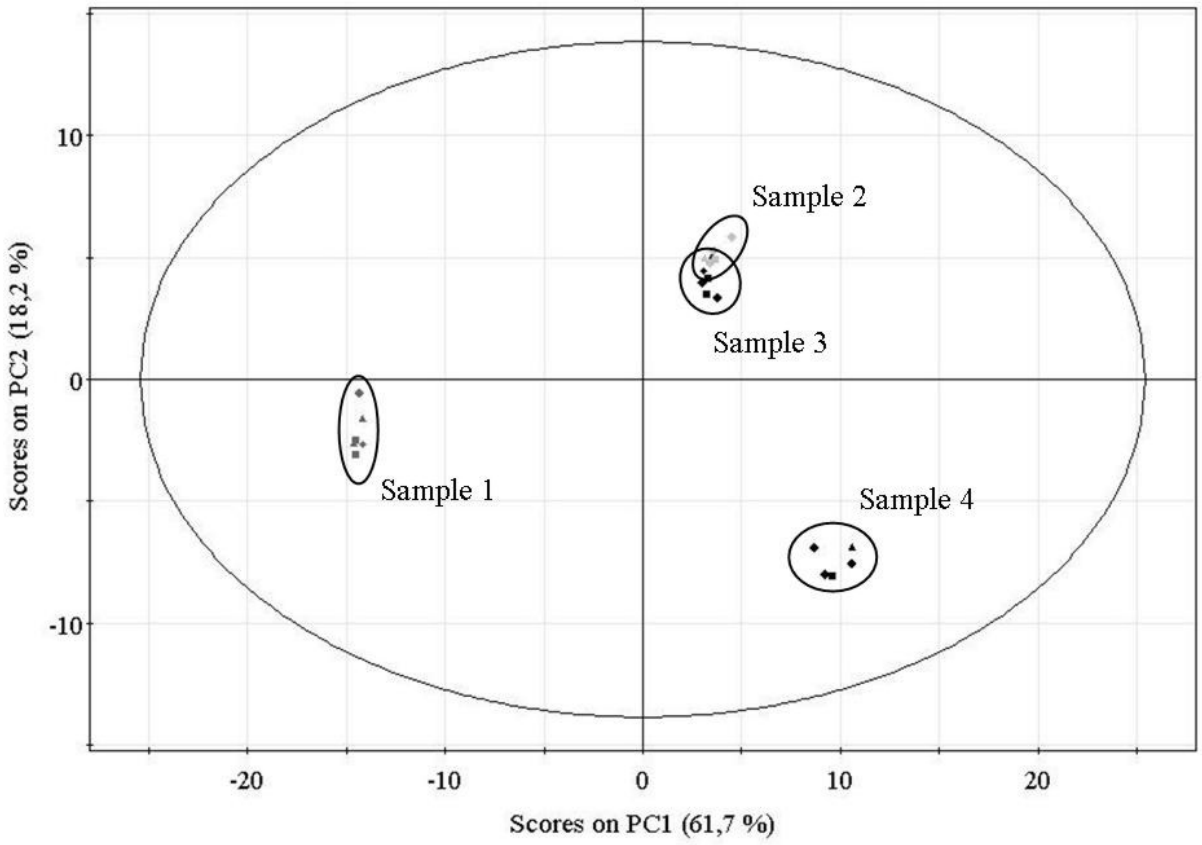
Sample 2
Sample 3
Sample 1
Sample 4
10
0
-10
-20
-10
0
10
20
Scores on PC2 (18,2 %)
Scores on PC1 (61,7 %)

Figure 6

Scheme

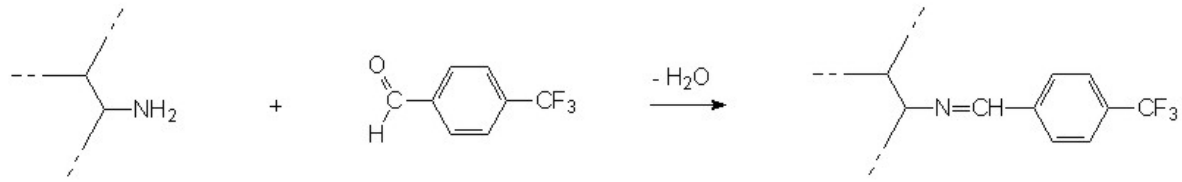

Scheme 1

List of Tables

Sample number	Power conditions	Plasma mode	Equivalent power conditions
1	150 W (peak power) – 20 % (duty cycle)	Pulsed	30 W
2	225 W (peak power) – 33 % (duty cycle)	Pulsed	75 W
3	75 W	CW	75 W
4	175 W	CW	175 W

Table 1

Equivalent power conditions	**Elemental composition of the derivatized-PPF**				$\%NH_2$ (%)	I_{allyl} (arbit.units)
	[C] (%)	[N] (%)	[O] (%)	[F] (%)		
30 W – Pulsed	72.8	14.2	4.3	8.7	20,4	270
75 W – Pulsed	78.3	15.1	2.7	3.9	8,6	30
75 W – CW	78.4	15.2	2.5	3.9	8,5	35
175 W – CW	80.1	14.6	2.4	2.9	6,6	5

Table 2

Negative loadings of PC1			*Positive loadings of PC1*		
$C_7H_{12}^+$	$\mathbf{C_9H_{13}N^+}$	$\mathbf{CH_4N^+}$	$C_3H_3^+$	$C_2H_3^+$	$C_5H_4^+$
$C_7H_{11}^+$	$C_8H_{12}^+$	$\mathbf{C_3H_7N^+}$	$C_4H_3^+$	$C_5H_5^+$	CH_3^+
$C_6H_{10}^+$	$C_6H_{11}^+$	$C_4H_8^+$	$C_6H_5^+$	$C_5H_2^+$	$C_{11}H_9^+$
$\mathbf{C_5H_{10}N^+}$	$C_9H_{13}^+$	$C_9H_{12}^+$	$C_3H_2^+$	$C_{10}H_8^+$	$C_6H_3^+$
$C_5H_{10}^+$	$C_9H_{14}^+$	$\mathbf{C_2H_6N^+}$	$C_5H_3^+$	$C_4H_5^+$	CHO^+
$C_8H_{13}^+$	$C_7H_{10}^+$	$C_8H_{11}^+$	$C_3H_5^+$	$C_4H_2^+$	$C_3H_4^+$
$\mathbf{C_3H_8N^+}$	$\mathbf{C_4H_6N^+}$	$\mathbf{NH_4^+}$	$C_2H_2^+$	$C_9H_7^+$	C_2H^+

Table 3

Negative loadings of PC2			*Positive loadings of PC2*		
$C_{10}H_{13}^+$	$C_2H_3O^+$	$C_5H_{11}^+$	$C_{15}H_{14}^+$	$C_{14}H_{12}^+$	$C_{11}H_8^+$
$C_5H_9^+$	$C_4H_7^+$	CHO^+	$C_8H_8^+$	$C_{10}H_{10}^+$	$C_{13}H_{11}^+$
$C_3H_5O^+$	$C_2H_4^+$	CH_3^+	$C_{13}H_{12}^+$	$C_{14}H_{13}^+$	$C_{16}H_8^+$
C^+	CH_3O^+	$C_3H_6^+$	$C_{15}H_{13}^+$	$C_{13}H_{13}^+$	$C_{15}H_{10}^+$
$C_6H_{13}^+$	CH_2^+	$C_3H_4^+$	$C_{16}H_{12}^+$	$C_9H_{10}^+$	$C_{15}H_{12}^+$
CH^+	$C_3H_7^+$	$C_4H_9^+$	$\mathbf{C_4N^+}$	$\mathbf{C_4HN^+}$	$C_{12}H_{13}^+$

Table 4

Figure captions

Figure 1. Experimental Set-up - 1: introduction airlock; 1': substrate holder; 2: slide valves; 3: water-cooled radiofrequency copper coil; 4: optical spectrometer; 4': optical fibre; 4": collimator network; 5: mass spectrometer; 6: organic precursor inlet; 7, 7': turbomolecular pump and throttle valve; 8: rotary pump; 9: Baratron gauge; 10: tap valves.

Figure 2. (a) Electron impact mass spectrum of allylamine vapor, (b-e) RGA mass spectra of allylamine plasma varying the P_{eq} conditions.

Figure 3. Typical XPS survey spectra of allylamine plasma polymer films (a) as-deposited and (b) TFBA-derivatized.

Figure 4. $\%NH_2$ as a function of the derivatization duration (the dotted lines are added to guide the eye in underlining the time at which the reaction is complete).

Figure 5. Positive ToF-SIMS spectra of the allylamine PPF varying the P_{eq} conditions.

Figure 6. "Scores plot" of the PPF showing samples separation according to PCA analysis of the ToF-SIMS data.

Scheme title

Scheme 1. Chemical gas-phase reaction occurring during TFBA derivatization of the PPF – NH_2 groups.

Table titles

Table 1. Experimental conditions under which allylamine PPF were synthesized.

Table 2. Elemental chemical composition and *%NH₂* of the PPF with regard to the precursor RGA signal in the plasma (I_{allyl}) varying the P_{eq} conditions.

Table 2. PC1 negative and positive loadings. The characteristic ionized fragments are hydrocarbonated ($C_xH_y^+$), nitrogen-based ($C_xH_yN^+$) and, at a lesser extent, oxygen-based ($C_xH_yO^+$). The latter are likely the result of post-growth oxidation processes following samples exposure to atmosphere.

Table 3. PC2 negative and positive loadings. The ionized fragments are hydrocarbonated ($C_xH_y^+$), nitrogen- ($C_xH_yN^+$) and oxygen-based ($C_xH_yO^+$).

Text for the "Table of Contents"

Plasma-polymerized surfaces presenting high primary amines concentration are of importance for many biomedical applications. We have studied the plasma polymerization of allylamine by correlating mass spectrometry diagnostic with the chemical composition (XPS/TFBA derivatization) and cross-linking degree (ToF-SIMS/PCA) of the films. We have demonstrated that these features depend directly on the equivalent RF power injected in the plasma but are not affected by the plasma mode used (pulsed or continuous wave).

Graphic for the "Table of Contents"